Bulgarian Chemical Communications, Volume 58, Issue 4 (pp. 442-450) 2026 *DOI: 10.34049/bcc.58.4.5740*

Photocatalytic degradation of azo dye (Congo red) using aluminum-doped cadmium oxide nanoparticles

M. S. Deshpande[1], D. V. Sonawane[1*], S. S. Deshmukh[1], A. E. Athare[2]

[1]*Department of Chemistry, Pemraj Sarda College, Ahilyanagar, (MS), India*
[2]*New Art's Commerce and Science College, Ahilyanagar, (MS), 414001, India*

Received: December 26, 2025; Revised: June 25, 2026

In this work, cadmium oxide (CdO) nanoparticles doped with aluminum (Al) at various amounts (0.002, 0.004, 0.006, and 0.008 g) were made by sol-gel citrate synthesis. X-ray diffraction (XRD), Fourier transform infrared spectroscopy (FTIR), ultraviolet-visible (UV-Vis) spectroscopy, scanning electron microscopy (SEM), and energy-dispersive X-ray spectroscopy (EDS) were used for chemical and elemental characterization. The organic dye was degraded using Al-doped CdO NPs, and the catalysis was assessed by UV-Vis absorption spectrometry. Finally, it was proven that these nano-catalysts destroyed the organic dye at an amount of 0.008 g with 93% degradation efficiency in 90 min. Al-doped CdO NPs may therefore be employed as catalysts to remediate industrial effluents.

Keywords: cadmium oxide nanoparticles, aluminum, EDS, SEM, azo dye.

INTRODUCTION

A variety of methods including coagulation, flocculation, membrane filtration, photo-catalytic degradation, etc., have been used to remove colored contaminants from textile, food, paper, cosmetics, and other industries releasing toxic contaminants into the environment. The textile industry's discharged wastewater is mostly polluted with dyes that deplete oxygen and harm aquatic life [1]. Congo red (CR) is an extensively used synthetic dye. It is a crucial model contaminant for assessing how well nanotechnology works to clean wastewater. Furthermore, researchers employ CR as a dopant to improve the catalytic, thermal, and optical characteristics of particular host nanoparticles. CR acts as a target for nanoparticle adsorption and degradation [2]. The development of nanoscience and nanotechnology has made it possible to produce nanoparticles using a variety of methods. Researchers have looked into numerous semiconductors that use visible light to break down a lot of resistant chemicals in aqueous systems; in fact, nano-sized metal oxide semiconductor materials are now widely acknowledged as the best substances for water purification [3]. Many metal oxide semiconductors including ZnO [4], SnO_2 [5], TiO_2 [6], metal particles such as Ag [7], Au [8], Pd [9], Pt [10], and a few doped metal oxides [11] have been extensively utilized to break down organic contaminants, e.g. methylene blue [12]. La-doped ZnO nanoflowers [13], Ag-doped CdO nanocomposite [14], and polyaniline CdO nanocomposite [15]. To the best of our knowledge, however, no reports have yet been made on the synthesis of Al-doped CdO nanoparticles and their particle size-related photo-catalytic activity in the photo-degradation of CR. Therefore, the goal of the current work was to investigate the photo-catalytic degradation of CR dye using an Al-doped CdO photo-catalyst produced by the chemical co-precipitation approach using the sol-gel citrate method.

Materials and methods

Al-doped CdO nanoparticles were produced by chemical co-precipitation using the sol-gel citrate method. For this purpose, citric acid, ethylene glycol, muffle furnace, aluminum nitrate hexahydrate [(Al $(NO_3)_2.6H_2O$)] and cadmium nitrate tetrahydrate [Cd $(NO_3)_2.4H_2O$] were used. All chemicals were of analytical grade.

A scanning electron microscope (SEM), JEOL JSM-5910 was used to examine the morphology of CdO nanoparticles (NPs). Energy-dispersive X-ray (EDX) spectroscope model INCA 200 was used to examine the elemental composition of the synthesized Al-doped CdO nanoparticles. The particle size and the group frequencies of the latter were examined using XRD (DW-XRD-Y3000) and FTIR (Bruker ALPHA II Compact FTIR) technique from Savitribai Phule, Pune University.

* To whom all correspondence should be sent: Email: *dvsonawane011@gmail.com*

© 2026 Bulgarian Academy of Sciences, Union of Chemists in Bulgaria

Synthesis of Al-doped CdO nanoparticles

Nanocrystalline pure and Al-doped CdO nanoparticles were synthesized by employing the sol-gel citrate technique. A stoichiometric mixture of cadmium nitrate tetrahydrate (Cd $(NO_3)_2.4H_2O$) with citric acid and ethylene glycol was appropriately blended. The mixture was agitated on a magnetic stirrer at 80°C for 3 h to obtain a homogenous transparent solution. To create a gel, the mixture was further heated in a pressure vessel at 130° C for almost 12 h. Then the gel was exposed to heat treatment at 350°C in a muffle furnace to get a fine dry powder of pure CdO nanoparticles. The same procedure was performed for Al-doped CdO nanoparticles using aluminum nitrate hexahydrate, [(Al $(NO_3)_2.6H_2O$)] to create $Al_xCd_{1-x}O$ nanoparticles.

RESULTS AND DISCUSSION

Characterization and structural analysis of the synthesized Al-doped CdO NPs were performed by XRD, FTIR, UV, SEM, and EDX analysis discussed below.

Structural analysis

XRD analysis: The generated Al-doped CdO nanoparticles of varied concentration were characterized using X-ray diffraction to gather information on crystal structure, crystallite size and purity. XRD patterns of the produced cadmium oxide and doped cadmium oxide were obtained at ambient temperature. The scanning angle 2θ was adjusted in the range of 20-80°. X-ray diffraction data were acquired by employing Cu Kα radiation (1.5406 Å). The full width at half maximum of the peaks was used to calculate the crystallite size of the generated pure CdO and Al-doped CdO nanostructures using the Scherrer formula [16].

$$d = \frac{K\lambda}{\beta \mathrm{Cos}\theta} \qquad (1)$$

where d is the average crystallite grain size; β is the full width half maximum in radian; θ is the Bragg angle; λ is the wavelength of X-rays (0.15406 nm for Cu target Kα radiation); K is a shape factor.

Two distinctive peaks are visible in the XRD patterns shown in Figures 1a and 1b. The peaks in Figure 1a are regarded as fingerprints for a highly polycrystalline pure CdO compound without visible presence of aluminum oxide. The use of a very tiny quantity of Al as a dopant is the reason for the lack of aluminum oxide peaks. The (111) and (200) planes contain the Al: CdO film's highest intensity peaks. As a result, these crystallographic planes have the ideal orientation for crystal formation. The degree of crystallization for the plane (111) is slightly higher. The increased crystallinity can be attributed to the films being on the hot plate for a few hours following deposition (annealing process), which eliminates the internal tensions caused by alternate spraying. The typical XRD spectra of pure and doped CdO nanoparticles at 650° C are shown in Figures 1a and 1b, respectively. The produced single-phase CdO nanoparticles show a rock salt-like cubic crystal structure with unit cell parameters, a = b = c = 4.6990 Å and α = β = γ = 90°. The corresponding reflection peaks of (hkl) are seen at (111), (200), (220), (311), and (222). The XRD peaks in the (111) crystallographic plane of CdO nanoparticles are crisp, confirming the nanoparticles' crystalline structure [17]. The crystallinity of the doped nanoparticles decreases with rise in the doping %, as shown in Table 1.

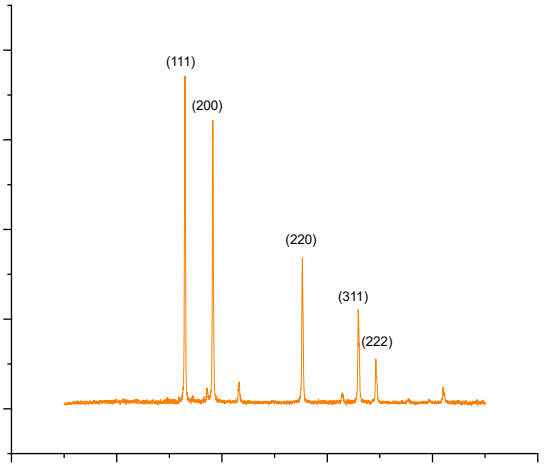

Figure 1a. XRD spectrum of undoped CdO NPs.

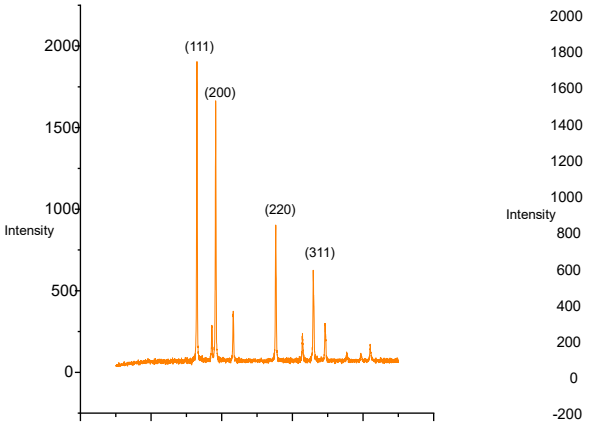

Figure 1b. XRD spectrum of Al-doped CdO NPs.

Table 1. Particle sizes in Al-doped CdO nanoparticles.

Samples	Particle size (nm)	Lattice parameter (Å)
CdO: nanoparticles	38.20	4.7990
CdO: Al (0.2%)	40.9	4.2786
CdO: Al (0.4%)	36.0	4.2771
CdO: Al (0.6%)	31.15	4.7446

Fourier transform infrared spectroscopy (FTIR) analysis

The spectra of pure and Al-doped CdO nanoparticles were measured in the range from 500 to 4000 cm^{-1}. It was noticed that owing to atmospheric moisture, the O-H stretching vibrations occurred around 3742.90 cm^{-1}. The CdO stretching was corroborated by the absorption peak at 2408 cm^{-1} and that at 2356 cm^{-1} was assigned to asymmetric CH_2 stretching frequency. FTIR also reveals the presence of O-H and Cd-O vibrations, as seen in Figures 2a and 2b [18].

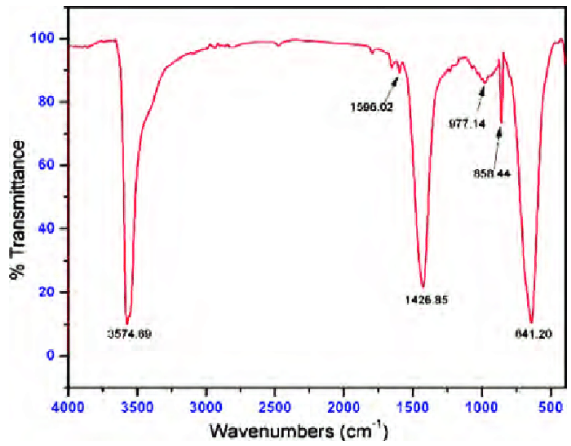

Figure 2a. FTIR spectrum of undoped CdO NPs.

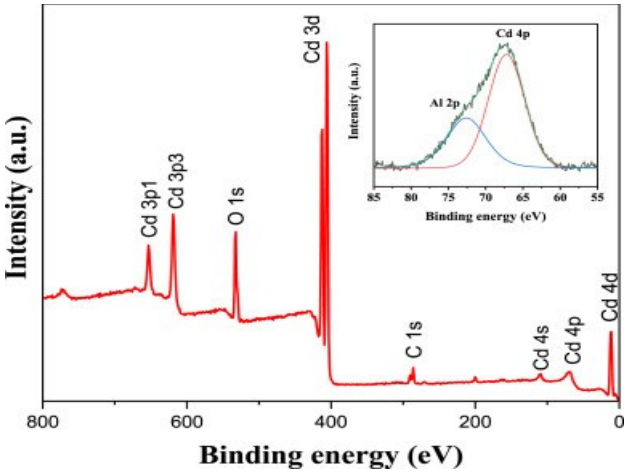

Figure 2b. FTIR spectrum of Al-doped CdO NPs.

UV- visible spectroscopy analysis

The band gap of Al-doped CdO nanoparticles is usually wider than that of undoped CdO. Undoped CdO is an n-type semiconductor with an intrinsic direct band gap spanning between 2.2 eV and 2.5 eV, as shown in Figure 3a. When doped with Al, the band gap changes upward depending on the dopant concentration, generally reaching between 2.5 eV and 3.0 eV. Two events are the main causes of the band gap difference between undoped and Al-doped CdO NPs. The absorption spectrum of Al-doped CdO NPs demonstrates that CdO NPs absorb in the range of 250-500 nm, which suggests that the CdO sample absorbs light in the visible range. The absorption spectrum at around 280 nm which is related to the electronic transition suggests that the CdO NPs were correctly synthesized [19]. The result is presented in Figure 3b.

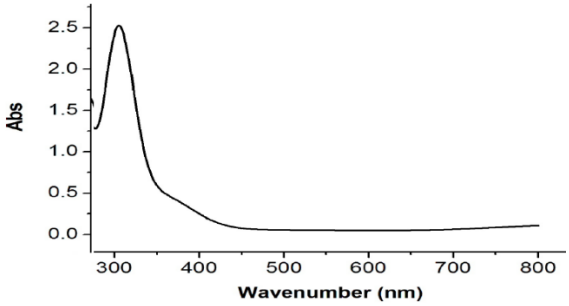

Figure 3a. UV-Vis spectrum of pure CdO NPs.

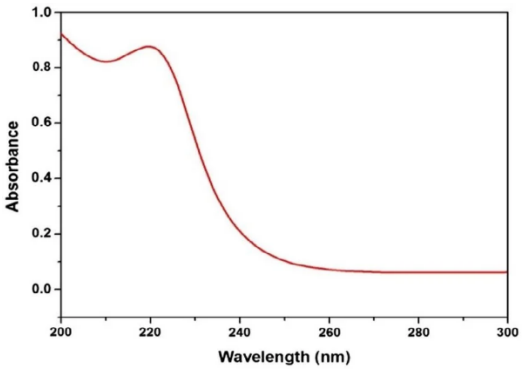

Figure 3b. UV-Vis spectrum of Al-doped CdO NPs.

Causes for the increase in band gap

Burstein-Moss (BM) effect: Aluminum functions as n-type donor in cadmium oxide because it is a trivalent metal. By substituting Cd, Al adds more free electrons to the conduction band. This effectively increases the optical band gap by filling the lowest accessible energy levels in the conduction band and making electrons need higher energies to migrate from the valence band.

Quantum confinement effect: Doping frequently inhibits nanoparticle development, resulting in reduced crystallite sizes. Spatial confinement of charge carriers results in a blue-shift in the

absorption spectra below a crucial threshold, which increases the band gap.

SEM analysis

The surface morphology of the samples was investigated using scanning electron microscopy. Figure 4a depicts the morphology of undoped CdO samples, which suggests that there is a spherical grain aggregation while Al-doped CdO nanoparticles have a somewhat corn-like nanorod shape shown in Figure 4b [20]. SEM images reveal that pure CdO is more crystalline and has ball-like structure. By Al-doping, the structure becomes nanowire and the diameter decreases with the increase in Al concentration, as seen in Figure 4b.



Figure 4a. SEM image of pure CdO NPs.

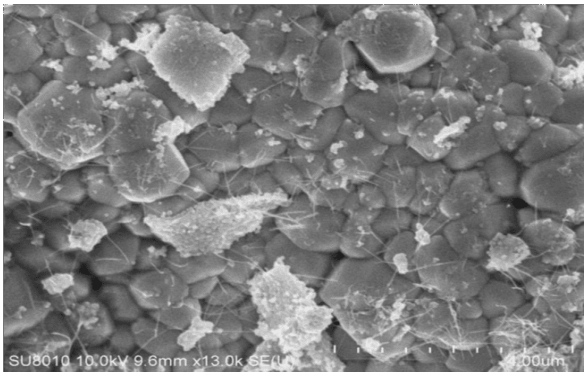

Figure 4b. SEM image of Al-doped CdO NPs.

EDS analysis

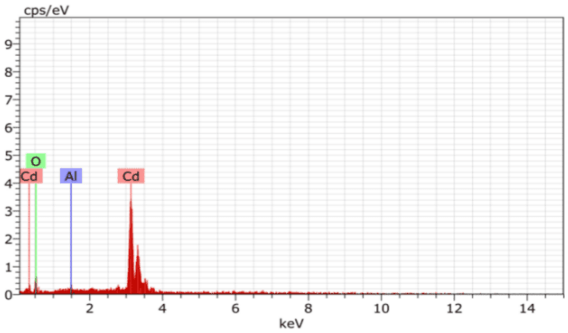

Figure 5. EDS image of Al-doped CdO NPs.

The EDS image of Al-doped CdO NPs reveals the presence of Al and no other impurities. Numerous distinct peaks related to Al, O, and Cd are visible in the EDX spectrum. The absence of additional impurity-related peaks in the spectrum further verifies that the produced nanoparticles are of Al-doped CdO, as shown in Figure 5 [21].

Photocatalytic degradation of Congo red dye

CR dye was catalytically degraded in aqueous media under UV irradiation to evaluate the photo-catalytic activity of the Al-doped CdO nanoparticles created in this investigation. Photographs of a CR dye solution taken at different time intervals (15, 30, 45, 60, 75, and 90 min, see Figure 6a) were used to visualize the degradation process. The color shifts seen in the images offer a tangible proof of the CR dye's gradual photo-degradation. In particular, a discernible rise in dye degradation is correlated with a progressive increase in irradiation time. CR distinctive color is more noticeable at the earlier time points, suggesting a larger dye concentration in the solution.

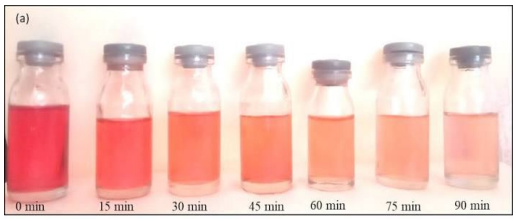

Figure 6a. CR dye degradation in solution taken at different time intervals.

The photo-catalytic system's effectiveness over prolonged irradiation times is highlighted by these visual observations, which are consistent with the quantitative analysis of the photo-catalytic degradation process and confirm that the synthesized Al-doped CdO NPs show a time-dependent enhancement of their ability to degrade CR dye [22]. By tracking the relative intensity of the UV-Vis spectral peak linked to CR, the photo-degradation of CR was evaluated at 497 nm (see Figure 6b). The proportion of CR dye degradation over time is shown in Figure 6c. The graph clearly shows that degradation is slowing with time. In particular, the following percentages of dye degradation are noted: 33% at 15 min, 50% at 30 min, 66% at 45 min, 83% at 60 min, 86% at 75 min, and 93% at 90 min. These findings imply that the photo-degradation of CR is a time-dependent process, where a longer duration results in more significant dye degradation [23].

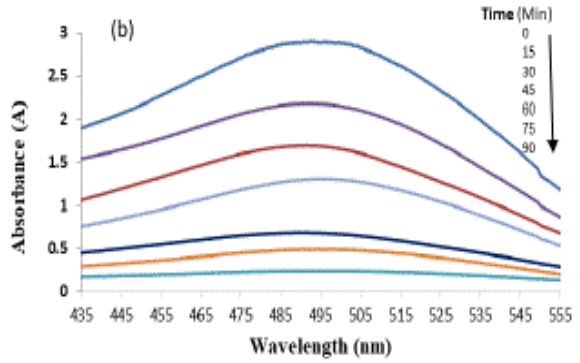

Figure 6b. UV-Vis spectral peak of CR dye solution.

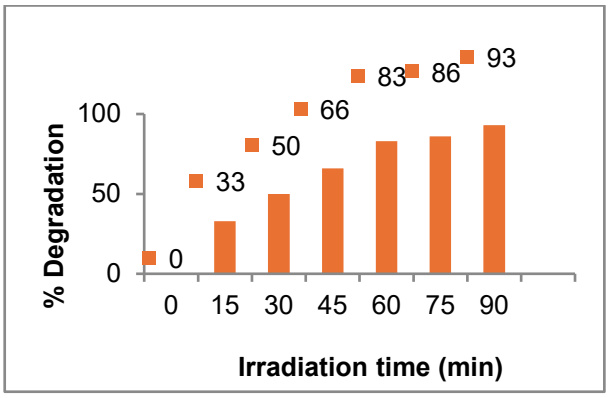

Figure 6c. Proportion of CR dye degradation over time.

Effect of dye concentration on photocatalytic degradation

The effect of dye concentration on the photo-catalytic degradation was investigated by keeping the amount of catalyst constant for 20 min. When the concentration of dye increased, the photo-degradation decreased, as shown in Figure 7a. The Beer-Lambert law which states that increased dye concentrations cause entering photons to travel a shorter distance, can be used to explain this tendency. As a result, there is less photon adsorption on the catalyst surface, which lowers the possibility of photo-degradation. The percentage of CR dye degradation is shown in Figure 7b, which shows a decrease as the dye concentration increases. For dye solutions containing 70, 80, and 90 parts per million of dye, the percent degradation during a 20-min period is 50%, 33%, and 11%, respectively (see Figure 7c). This result highlights the inverse relationship between dye concentration and photo-catalytic degradation efficiency, offering important information about how to maximize dye removal conditions [24].

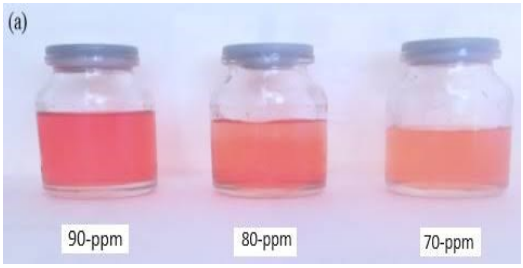

Figure 7a. Effect of dye concentration in solution on photo-catalytic degradation of CR dye.

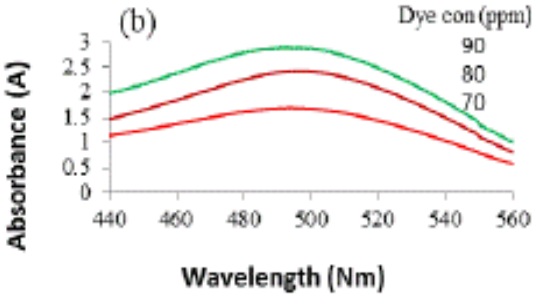

Figure 7b. Validity of Beer's law in CR dye degradation.

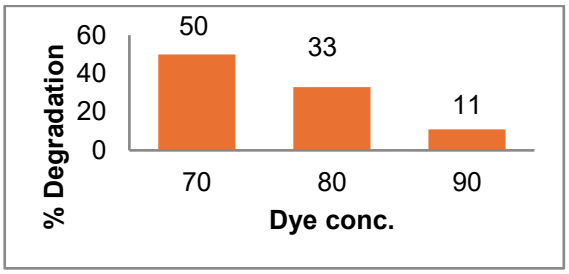

Figure 7c. Percent degradation of CR dye.

Effect of pH on the photo-degradation

Considering the variety of pH levels at which industrial effluents, especially those from industries like dyes, paints, and textiles, are usually released, the impact of pH on the photo-degradation of CR becomes an important issue. A thorough investigation of how pH affects the photo-degradation process is required due to the fluctuation in pH values in these effluents. The photo-degradation rates of CR dye show a clear dependence on pH of the medium, as seen in Figure 8. This relationship emphasizes how important pH is in determining the production of hydroxyl radicals and the overall photo-degradation effectiveness. The graph shows a positive correlation between pH and the rate of photo-catalytic degradation, with a discernible rise in degradation as the pH increases. Higher pH values cause an increase in the production of active hydroxyl radicals (•OH), which accelerates the pace of breakdown. The graphs in Figure 8 show that as pH rises, the percent deterioration proportionally increases. In particular, the percent degradation at

pH 4, 7, and 10 after 45 min is 46%, 60%, and 80%, respectively. The effect of pH on the production of hydroxyl radicals is responsible for the reported pH-dependent enhancement in the photo-degradation process. A more effective breakdown of the CR dye is made possible by the increased availability of hydroxyl radicals at higher pH values. This knowledge is essential for developing customized and efficient wastewater treatment methods by adjusting the photo-degradation process according to the unique pH conditions of industrial effluents [24, 25].

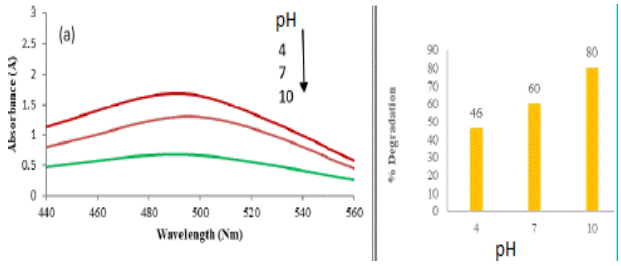

Figure 8. Positive correlation between pH and the rate of photo-catalytic degradation of CR dye.

Effect of the catalyst dosage on the photo-degradation

At a constant period of 20 min, the effect of catalyst dosage on the photo-degradation rate of CR dye was examined over a range of catalyst amounts, from 0.002 g to a maximum of 0.008 g per 20 mL of dye solution, as presented in Figure 9a. To explore the quantitative aspect, the percent UV degradation of CR dye during a 15-min period using varying concentrations of the photo-catalyst is presented in Figure 9b. The evolution of CR degradation in aqueous media with varying catalyst concentrations is graphically depicted in Figure 9c. For catalyst quantities of 0.002 g, 0.004 g, 0.006 g, and 0.008 g, the corresponding percent degradation values are 33%, 46%, 64%, and 75%, respectively. Higher catalyst amounts may result in better treatment outcomes, since this data supports the positive link between catalyst dosage and the effectiveness of CR dye degradation [26].



Figure 9a. Effect of catalyst dosage on CR dye degradation.

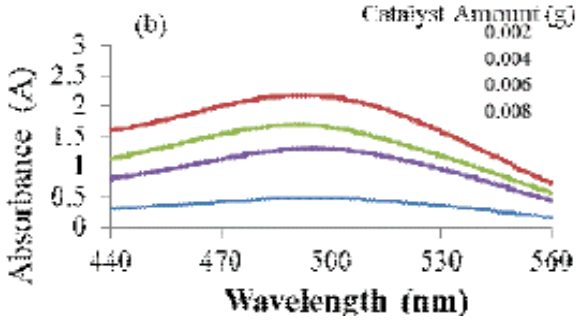

Figure 9b. Percent UV degradation of CR dye.

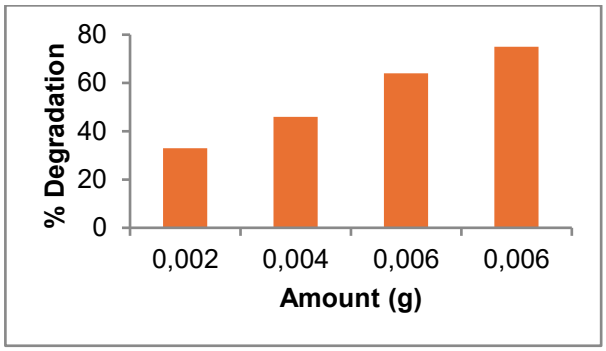

Figure 9c. Effect of catalyst dosage on the photo-degradation of CR dye.

Effect of the recovered catalyst on photo-degradation

The study highlights how the recovery procedure affects the catalyst photo-degradation activity. Recovery is important for cost-effectiveness and sustainability and is also critical to carefully analyze the change in catalyst performance. The observed decrease in photo-degradation efficiency emphasizes the necessity for additional recovery method improvement to preserve or improve the catalyst effectiveness in later applications. In order to evaluate the efficacy of recovered catalysts, the photo-degradation performance of the catalyst was investigated under standard experimental conditions. To guarantee that any adsorbed dye on the catalyst was removed, the recovery process required many washings with deionized water. The recovered catalyst showed a significant decrease in activity when compared to the original catalyst, even though it had a great capacity to degrade CR dye. The possible blockage of active sites on the photo-catalyst surface is responsible for the observed decrease in the recovered catalyst's photo-degradation efficacy, as shown in Figure 10a. The accumulation of photosensitive hydroxides during the heating process is the cause of this obstacle. These hydroxides may accumulate on the catalyst surface, impairing its capacity to effectively start photo-degradation reactions. The percent degradation of

CR dye by the original and the recovered photo-catalyst is graphically shown in Figure 10b. It is seen that during the 90-min experiment, the original catalyst accomplished amazing 93% dye degradation. The restored catalyst performed worse, degrading 82% of the dye for the same duration. The recovered catalyst's decreased activity is caused by a number of circumstances. Although washing procedures are necessary to remove adsorbed dye, they may unintentionally change the catalyst's surface characteristics and structural integrity. Furthermore, the catalyst's photo-degradation efficacy may be impacted by residual impurities or compositional changes that occur throughout the recovery process [27, 28].

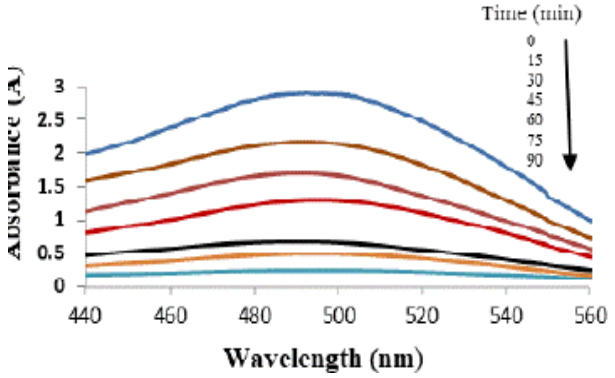

Figure 10a. Effect of the recovered catalyst on the photo-degradation of CR dye.

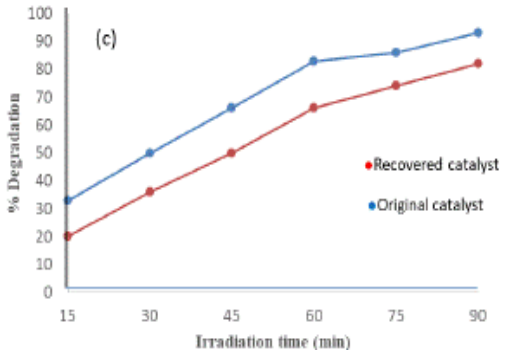

Figure 10b. Percent degradation of CR dye.

Mechanism of photocatalytic degradation and analysis of band gap energy

The suggested process of photo-catalytic degradation of the targeted CR dye is shown in Figure 11. The following mechanism underlies the photo-catalytic degradation of dyes: an electron-hole pair is created when the catalyst is activated by UV light, moving electrons from the valence band to the conduction band.

$$\text{Catalysts (NPs)} + h \rightarrow \text{NPs } (e^- + h^+) \quad (2)$$

The electron in the conduction band is represented by e^-, and the positive hole in the valence band is represented by h^+. These two species move to the catalyst surface, where they engage with other organic species. Because of its high oxidative potential, the positive hole can either directly oxidize the dye molecule or combine with water molecules to form hydroxyl radicals. Superoxide radicals, which are extremely reactive and aid in the deterioration of dyes, are created when electrons in the conduction band react with oxygen molecules [29]. The following equations provide a summary of the potential reactions.

$$\text{NPs} + h\nu \rightarrow \text{NPs } (h^+ + e^-) \quad (3)$$

$$h^+ + \text{dye} \rightarrow \text{oxidation of the dye molecules} \quad (4)$$

$$h^+ + OH^- \rightarrow \cdot OH \quad (5)$$

$$e^- + O_2 \rightarrow \cdot O_2 \quad (6)$$

$$\cdot OH + \cdot O^{2-} + \text{dye} \rightarrow \text{degradable/less toxic species} \quad (7)$$

An important consideration in the context of photo-catalysis is the band gap. Electrons in the valence band may be stimulated to the conduction band when a material is exposed to light, particularly in the visible light spectrum, resulting in the creation of electron-hole pairs. Numerous applications, including photo-catalysis, depend on this mechanism. With a band gap of 2.7 eV [29], metal oxides are implied to absorb light mostly in the UV region, which limits their efficiency in using visible light for photo-catalysis. However, the material becomes more sensitive to visible light when doped with Al, which causes the band gap to drop to 1.3 eV.The Burstein-Moss effect usually causes the band gap energy of Al-doped CdO nanoparticles to increase, although structural flaws or strain might cause it to decrease at higher doping concentrations. In conclusion, Al-doping of CdO nanoparticles results in a decrease in band gap values, which improves visible light utilization, increases electron-hole pair creation, and eventually enhances the metal oxide nanoparticles' photo-catalytic performance, as shown in Figure 12 [9].

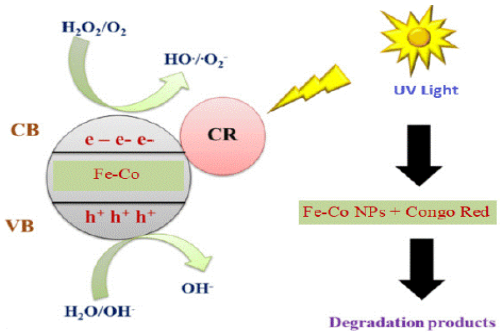

Figure 11. Mechanism of the photo-catalytic degradation of CR dye.

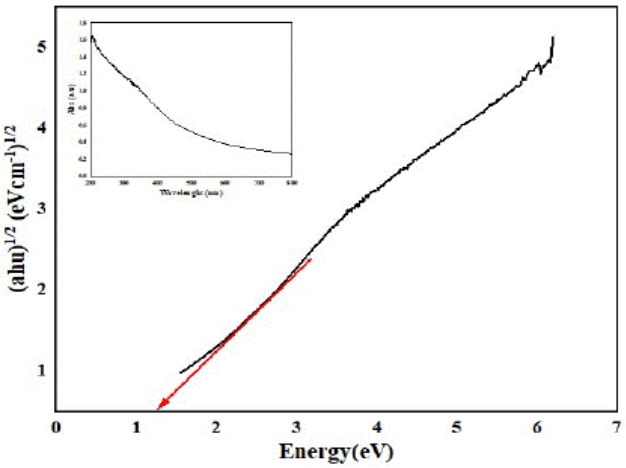

Figure 12. Band gap energy of Al-doped CdO NPs.

CONCLUSION

The results indicate that Al-doped CdO nanoparticles exhibit a notable level of photo-catalytic activity, particularly in the process of degrading Congo red dye through photo-degradation. Impressively, within a span of 90 min, a substantial 93% of the dye was successfully degraded. Notably, the observed trend reveals that as the duration of exposure increases, there is a corresponding augmentation in the photo-degradation of the dye. Furthermore, the study highlights the influence of the catalyst's quantity on the photo-degradation process. It was evident that an escalation in the amount of catalyst positively correlated with the degradation efficiency. For instance, utilizing 0.002 g of the photo-catalyst resulted in the degradation of 66% of the dye within a 45-min time frame. The impact of the medium's pH on the degradation process was also investigated. The findings illustrated a direct relationship between pH levels and dye degradation. Specifically, at pH 10, an impressive 80% of the dye underwent degradation within a relatively short span of 45 min, indicating the significance of the medium's alkalinity in enhancing the degradation efficiency. However, an intriguing observation emerged concerning the concentration of the dye. Surprisingly, the research demonstrated that as the concentration of the dye increased, the rate of photo-degradation exhibited a counter-intuitive decrease. This suggests a nuanced relationship between the dye concentration and the efficacy of the photo-degradation process.

Acknowledgement: *Authors are thankful to the Management and Principal of New Art's, Commerce and Science College, Ahilyanagar, for providing necessary facilities to the Department to carry out this work. Authors are also thankful to the Department of Physics Savitribai Phule Pune University, for characterization of samples.*

REFERENCES

1. K. A. Vijayalakshmi, N. Kartthikeyan, *Inorganic and Nano-Metal Chemistry,* ***55*****(6),** 657 (2024).
2. S. Krishnaraj, R. Anitha, *Journal of Advanced Scientific Research,* **12**(1), 0976-9595, 75 (2021).
3. H. Munawaroh, S. Wahyuningsih, A. H. Ramelan, *Materials Science and Engineering***, 176,** 012049, 1 (2017).
4. S. Sivakumar, N. Pallavi, S. Surendiran, P. Sangeetha, B. Karthikeyan, C. T. Manikandan. B. Sangeetha, E. B. Bharathi, *AIP Advances,* **16,** 045124, 1 (2026).
5. Sh. Mathur, R. Jain, *International Journal of Latest Technology in Engineering, Management and Applied Science (IJLTEMAS),* **8(12),** 28 (2019).
6. S. A. Muhammed, N. K. Abbas, *Baghdad Science Journal,* **20(5),** 2411 (2023).
7. N. H. Harb, H. Y. Hammod, S. T. Mohmmed, B. H. Adil, *Journal of Physical Science*, **35(3),** 17 (2024).
8. Sh. N. Matussin, F. Khan, M. H. Harunsani, Y.-M. Kim, M. M. Khan, *Catalysts,* **13(96),** 2 (2023).
9. F. Shan, L. Panariello, G. Wu, A. Gavriilidis, H. H. Fielding, I. P. Parkin, *RSC Adv.,* **11,** 17694 (2021).
10. A. Tabriz, N. Shahzad, S. Nadeem, S. Mehmood, N. Iqbal, G. Ali, M. I. Shahzad, *Mater. Proc.,* **17(9),** 2 (2024).
11. V. Aherkar, A. A. Mohammed, A. A. Al-shimary, R. M. Ovhal, Sh. Pawar, G. Kamblee, P. A. Ubale, *RSC Adv.,* **16,** 16253 (2026).
12. T. Alemu, G. Taye, G. Asefa, L. B. Merga, *Heliyon*, **8,** e11608 (2022).
13. E. S. Al-Farraj, E. A. Abdelrahman, *ACS Omega,* **9,** 4870 (2024).
14. M. S. Deshpande, D. V. Sonawane, Sh. S. Deshmukh, A. E. Athare, *Current Science,* **6(1),** 5846 (2026).
15. M. S. Deshpande, D. V. Sonawane, S. S. Deshmukh, and A. E. Athare, *International Journal of Scientific Research in Science, Engineering, and Technology*, **12(6),** 225 (2025).
16. D. V. Sonawane, *Science, Technology and Development*, **11(5),** 0950-0707, 388 (2022).
17. M. S. Deshpande, D. V. Sonawane, Sh. S. Deshmukh, A. E. Athare, *Journal of Scientific Research and Report,* **32(4),** 176 (2026).
18. H. H. Darwoysh, A. A. Yousif, K. A. Aadim, *International Journal of Scientific Research in Science and Technology,* **10(3),** 310 (2023).
19. R. A. Jassim, A. S. Abbas, *Iraqi Journal of Chemical and Petroleum Engineering*, **26(2),** 83 (2025).
20. S. Arul, T. Senthilnathan, *Rasayan J. Chem.,* **12(2),** 891 (2019).
21. L. K. Gaur, P. Gairola, S. P. Gairola, M. Ch. Mathpal, P. Kumar, S. Kumar, D. Kushavah, V. Agrahari, F. F. H. Aragon, M. A. G. Soler, H. C. Swart, *J. Alloys Compd.,* **868,** 159189 (2021).

22. D. T. Sponza, *American Journal of Surgery and Clinical Case Reports,* **6(16),** 1 (2023).
23. A. A. Manda, Q. A. Drmosh, Kh. A. Elsayed, A. L. Al-Alotaibi, I. O. Alade, S. A. Onaizi, H. D. M. Dafalla, A. Elhassan, *Arab. J. Chem.,* **15(8),** 104004 (2022).
24. S. Mondal, B. Bhattacharjee, *J. Water Environ. Nanotechnol.*, **9(4),** 415 (2024).
25. J. Panwar, L. Joshi, R. Ameta, D. Soni, *Rasayan J. Chem.,* **16(3),** 1326 (2023).
26. A. Krisandi, H. Harsono, N. Yudasari, *Trends Sci.,* **21(11),** 8219 (2024).
27. E. P. Soto, C. A. Rodriguez Gonzalez, P. A. Luque Morales, H. Reyes Blas, A. Carrillo Castillo, *Catalysts,* **14,** 589 (2024).
28. J. M. Thornton, D. Raftery, *ACS Appl. Mater. Interfaces*, **4(5),** (2012).
29. S. M. Albukhari, A. A. Ismail, *ACS Omega*, **6(36),** (2021).